144 *Inorg. Chem.* **2011**, *50*, 144–154
DOI: 10.1021/ic101488k

Inorganic Chemistry
Article

Hydrothermal Synthesis, Structures and Magnetic Studies of Transition Metal Sulfates Containing Hydrazine

Li-Hui Jia,[†,‡] Ru-Yin Li,[§] Zhi-Ming Duan,[†] Shang-Da Jiang,[†] Bing-Wu Wang,*[,†] Zhe-Ming Wang,[†] and Song Gao*[,†]

[†]*Beijing National Laboratory of Molecular Science, State Key Laboratory of Rare Earth Materials Chemistry and Applications, College of Chemistry and Molecular Engineering, Peking University, Beijing 100871, China,* [‡]*Key Laboratory for Green Chemical Process of Ministry of Education, School of Chemical Engineering and Pharmacy, Wuhan Institute of Chemical and Technology, Wuhan 430074, China, and* [§]*China National Offshore Oil Corporation Research Institute, State Key Laboratory of Offshore Oil Exploitation, Beijing, 100027, China*

Received July 25, 2010

By employing hydrothermal method, six transition metal sulfates containing hydrazine (N_2H_4) have been obtained: $[M(SO_4)_2(N_2H_5)_2]_n$ (M = Mn(**1**), Co(**2**), Ni(**3**)) and $[M(N_2H_4)SO_4]_n$ (M = Mn(**4**), Co(**5**), Ni(**6**)). Their crystal structures and magnetic properties have been investigated experimentally and theoretically. Compounds **1**−**3** consist of one-dimensional sulfate bridged homometallic chains with protonated hydrazine molecule as terminal ligand, and compounds **4**−**6** are hydrazing-sulfate mixed bridged homometallic three-dimensional frameworks. Compounds **1**−**6** exhibit antiferromagnetic coupling between M^{2+} ions, but their magnetic properties differ at low temperatures because of the different single-ion anisotropy and crystal structures. The magnetostructural correlations and the magnetic coupling mechanism are analyzed by density functional theory calculations (DFT).

Introduction

The design and synthesis of transition-metal complexes with short bridge ligands of one- to three-atom such as O^{2-}, CN^-, N_3^-, $HCOO^-$, and $C_2O_4^{2-}$ are currently under intense investigation in order to understand the structural and chemical factors governing the exchange coupling interaction between paramagnetic centers and to discover the new magnetic phenomena in molecular materials.[1,2] Generally, the shorter the bridges are, the more efficient the transmitting of magnetic coupling will be. Recently, we have obtained a series of three-atom bridged molecular magnetic systems (N_3^-, COO^-, and NCN^-) and studied their magnetostructural correlations experimentally and theoretically.[3] So far as two-atom bridged molecular magnetic systems are concerned, a large number of studies are reported on the transition metal coordination polymers containing cyanide (CN^-) or oximato ($N-O^-$) ligands, as well as some triazole and tetrazole coordination polymers with N=N two-atom bridge.[4] As a short two-atom bridge ligand, unsubstituted hydrazine (N_2H_4) has more diversified coordination modes in constructing coordination complexes. It can act as monodentate, bridging or bidentate ligand coordinating to transition metal ions as depicted in scheme 1. Moreover the ability of hydrazine to transmit magnetic coupling was scarcely investigated. To our knowledge, the crystal structures of transition metal complexes with unsubstituted hydrazine ligand were seldom reported.[5] In 2007, we presented the magnetic studies of a honeycomb-layered cobalt(II) coordination polymer using hydrazine as the cobridge with azide.[6] It is the first and only one magnetic research of the hydrazine bridged transition metal coordination compounds until now.

Herein, we report the hydrothermal synthesis, structures, and magnetism of transition metal sulfates with hydrazine,

*To whom correspondence should be addressed. E-mail: gaosong@pku.edu.cn (S.G.); wangbw@pku.edu.cn (B.-W.W.). Fax: (+86)10-6275-1708.

(1) (a) Ferlay, S.; Mallah, T.; Ouahes, R.; Veillet, P.; Verdaguer, M. *Nature* **1995**, *378*, 701–703. (b) Sato, O.; Lyoda, T.; Fujishima, A.; Hashimoto, K.; Okawa, H. *J. Am. Chem. Soc.* **1992**, *114*, 6974–6979. (c) Ribas, J.; Escuer, A.; Monfort, M.; Vicente, R.; Cortés, R.; Lezama, L.; Rojo, T. *Coord. Chem. Rev.* **1999**, *193*−*195*, 1027–1068.

(2) (a) Miller, J. S.; Manson, J. L. *Acc. Chem. Res.* **2001**, *34*, 563–570. (b) Salah, M. B.; Vilminot, S.; André, G.; Richard-Plouet, M.; Bourée-Vigneron, F.; Mhiri, T.; Kurmoo, M. *Chem.—Eur. J.* **2004**, *10*, 2048–2057. (c) Meyer, F.; Demeshko, S.; Leibeling, G.; Kersting, B.; Kaifer, E.; Pritzkow, H. *Chem.—Eur. J.* **2005**, *11*, 1518–1526. (d) Yuan, M.; Gao, S.; Sun, H. L.; Su, G. *Inorg. Chem.* **2004**, *43*, 8221–8223.

(3) (a) Wang, X. Y.; Wang, Z. M.; Gao, S. *Chem. Commun.* **2008**, 281–294. (b) Li, R. Y.; Wang, B. W.; Gao, S. *Inorg. Chem.* **2009**, *48*, 7174–7180. (c) Yuan, M.; Zhao, F.; Pan, F.; Wang, Z. M.; Gao, S. *Chem.—Eur. J.* **2007**, *13*, 2937–2952. (d) Hu, K. L.; Wang, Z. M.; Gao, S. *Chem.—Eur. J.* **2009**, *15*, 12050–12064.

(4) (a) Ohba, M.; Okawaa, H. *Coord. Chem. Rev.* **2000**, *198*, 313–328. (b) Atanasov, M.; Comba, P.; Hausberg, S.; Martin, B. *Coord. Chem. Rev.* **2009**, *253*, 2306–2314. (c) Chaudhuri, P. *Coord. Chem. Rev.* **2003**, *243*, 143. (d) Garcia, Y.; van Koningsbruggen, P. J.; Kooijman, H.; Spek, A. L.; Haasnoot, J. G.; Kahn, O. *Eur. J. Inorg. Chem.* **2000**, *2*, 307–314. (e) Ouellette, W.; Prosvirin, A. V.; Whitenack, K.; Dunbar, K. R.; Zubieta, J. *Angew. Chem., Int. Ed.* **2009**, *48*, 1–5.

(5) Heaton, B. T.; Jacob, C.; Page, P. *Coord. Chem. Rev.* **1996**, *154*, 193–229.

(6) Wang, X. T.; Wang, Z. M.; Gao, S. *Inorg. Chem.* **2007**, *46*, 10452.

 Published on Web 12/02/2010

Scheme 1. Possible Bonding Modes of Hydrazine: (a) Monodentate, (b) cis-Bridging, (c) trans-Bridging, and (d) Bidentate

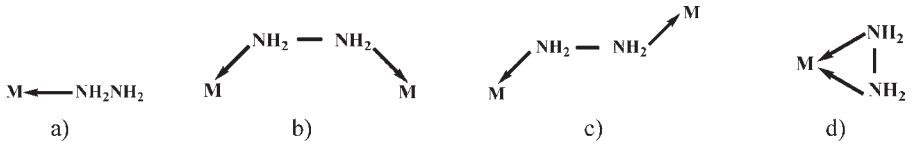

a) b) c) d)

$[M(SO_4)_2(N_2H_5)_2]_n$ (M = Mn(**1**), Co(**2**), Ni(**3**)) and $[M(N_2H_4)SO_4]_n$ (M = Mn(**4**), Co(**5**), Ni(**6**)). As far as we know, it is reported for the first time that the transition metal sulfates containing hydrazine are prepared by hydrothermal method. Although these six transition metal complexes consist of hydrazine and sulfate ligands only, they reveal different structures and magnetic properties because of the diversity modes of bridges. Compounds **1**−**3** are isomorphous one-dimension (1D) infinite chains and compounds **4**−**6** are isomorphous three-dimension (3D) compounds. The ability of hydrazine as bridge ligand in constructing structures and transmitting magnetic coupling are investigated. Density functional theoretical (DFT) calculations have been performed on model structures of **3·Ni** and **4·Mn** to investigate the magneto-structural correlations.

Experimental Section

General Materials. All starting materials were commercially available at analytical grade and used as purchased without further purification. The ligand 3-(1,2,4-triazolyl-4-yl)-1,2,4-triazole (Btr) was prepared according to the literature method.[7]

Preparations of 1D compounds $[M(SO_4)_2(N_2H_5)_2]_n$ (M = Mn (1), Co (2), Ni (3)). Method A: $MSO_4 \cdot nH_2O$ (0.75 mmol, 0.127 g for M = Mn, 0.211 g for M = Co and 0.197 g for M = Ni), Btr (0.5 mmol, 0.078 g) and HF 0.15 mL were mixed with 10.0 mL H_2O and 5.0 mL C_2H_5OH in a 25 mL Teflon-lined stainless-steel autoclave. The mixture was heated at 180 °C for 5 days in a furnace and naturally cooled to obtain suitable crystals. **Method B**: $MSO_4 \cdot nH_2O$ (0.5 mmol, 0.085 g for M = Mn, 0.141 g for M = Co and 0.131 g for M = Ni), $N_2H_4 \cdot H_2O$ (hydrazine hydrate, 0.5 mmol, 0.025 g), and HF 0.10 mL were mixed with 10.0 mL H_2O and 5.0 mL C_2H_5OH in a 25 mL Teflon-lined stainless-steel autoclave. The mixture was heated at 160 °C for 3 days in a furnace and then naturally cooled to obtain suitable crystals.

Yield of **1** based on **$MnSO_4$**: 35%. Elemental analysis calcd (%) for $N_4H_{10}S_2O_8Mn$: N 17.89, H 3.19, S 20.45; found: N 17.76, H 3.14, S 20.27. IR (cm^{-1}): 989 (m), 1005 (s), 1080 (vs), 1118 (vs), 1505 (s), 1576 (m), 1614 (m), 1637 (m), 2954 (m), 3073 (m), 3238 (s), 3292 (s).

Yield of **2** based on **$CoSO_4$**: 46%. Elemental analysis calcd (%) for $N_4H_{10}S_2O_8Co$: N 17.67, H 3.16, S 20.19; found: N 17.48, H 3.11, S 20.24. IR (cm^{-1}): 988 (m), 1014 (s), 1075 (vs), 1120 (vs), 1501 (s), 1577 (m), 1607 (m), 1629 (m), 2947 (m), 3073 (m), 3241 (s), 3296 (s).

Yield of **3** based on **$NiSO_4$**: 34%. Elemental analysis calcd (%) for $N_4H_{10}S_2O_8Ni$: N 17.66, H 3.15, S 20.18; found: N 17.60, H 3.15, S 20.21.IR (cm^{-1}): 988 (m), 1024 (s), 1065 (vs), 1124 (vs), 1504 (s), 1575 (m), 1600 (m), 1627 (m), 2949 (m), 3073 (m), 3241 (s), 3293 (s).

Preparations of 3D compounds $[M(N_2H_4)SO_4]_n$ (M = Mn (4), Co (5), Ni (6)). Method A: The synthesis procedure is similar with the Method A in the preparation of 1D compounds **1**−**3** but without HF. $MSO_4 \cdot nH_2O$ (0.75 mmol, 0.127 g for M = Mn, 0.211 g for M = Co and 0.197 g for M = Ni) and Btr (0.5 mmol, 0.078 g) was mixed with 10.0 mL of H_2O and 5.0 mL of C_2H_5OH in a 25 mL Teflon-lined stainless-steel autoclave. The mixture was heated at 180 °C for 5 days in a furnace and then naturally cooled to obtain suitable crystals. **Method B**: The synthesis procedure is similar with the Method B in the preparation of 1D compounds **1**−**3** but without HF. $MSO_4 \cdot nH_2O$ (0.5 mmol, 0.085 g for M = Mn, 0.141 g for M = Co and 0.131 g for M = Ni), $N_2H_4 \cdot H_2O$ (hydrazine hydrate, 0.5 mmol, 0.025 g) were mixed with 10.0 mL of H_2O and 5.0 mL of C_2H_5OH in a 25 mL Teflon-lined stainless-steel autoclave. The mixture was heated at 160 °C for 3 days in a furnace and then naturally cooled to obtain suitable crystals.

Yield of **4** based on MnSO4: 52%. Elemental analysis calcd (%) for $N_2H_4SO_4Mn$: N 15.30, H 2.19, S 17.48; found: N 15.37, H 2.21, S 17.40. IR (cm^{-1}): 627 (m), 641 (m), 1092 (vs), 1111 (vs), 1584 (m), 1590 (m), 1639 (w), 3190 (w), 3275 (m), 3312 (m), 3324 (s).

Yield of **5** based on CoSO4: 67%. Elemental analysis calcd (%) for $N_2H_4SO_4Co$: N 14.97, H 2.14, S 17.11; found: N 15.10, H 2.07, S 17.15. IR (cm^{-1}): 636 (m), 654 (m), 1088 (vs), 1107 (vs), 1189 (m), 1200 (m), 1584 (m), 1592 (m), 1638 (w), 3190 (w), 3274 (m), 3307 (m), 3321 (s).

Yield of **6** based on NiSO4: 42%. Elemental analysis calcd (%) for $N_2H_4SO_4Ni$: N 14.95, H 2.14, S 17.09; found: N 14.85, H 2.36, S 17.21. IR (cm^{-1}): 667 (w), 1091 (vs), 1112 (vs), 1585 (m), 1594 (m), 1638 (w), 3189 (w), 3269 (m), 3303 (m), 3318 (s).

X-ray Crystallography and Physical Measurements. The crystallographic data for the single crystals of the six compounds (**1**−**6**) were collected at 293K on a Nonius KappaCCD diffractometer with a 2.0 kW sealed anode source using graphite monochromated $Mo_{K\alpha}$ radiation of λ = 0.71073 Å.[8] Empirical absorption corrections were applied using the Sortav program.[9] Because the crystals of compound **1** (M = Mn) and compound **6** (M = Ni) were always twined, only the structures of compounds **2**−**5** were well solved by direct methods and refined by full-matrix least-squares on F^2 using SHELX program.[10,11] All non-hydrogen atoms were refined anisotropically. Hydrogen atoms were added geometrically and refined using the riding model. The refined N−H distances, bond angles involving H atoms and isotropic thermal factors of H atoms are all of rational values. The details of data collection, data reduction, and crystallographic data are summarized in Table 1, selected bond lengths and angles in Table 2 and the data of hydrogen bonds in the Supporting Information.

PXRD data for compounds **1**−**6** were collected in the range of 5−50° for 2θ at room temperature against the bulk samples using a Rigaku Dmax 2000 diffractometer with $Cu_{K\alpha}$ radiation in flat-plate geometry. The identities of the bulk materials for compounds **1**−**6** were established by comparing the experimental observed powder X-ray diffraction (PXRD) patterns to the calculated ones from the single-crystal structures (Figure S1 in the Supporting Information). It should be mentioned that the simulated PXRD patterns of compound **1·Mn** and **6·Ni** are obtained from the present single-crystal data without refinement.

(7) Herbst, R. M.; Garrison, J. A. *J. Org. Chem.* **1953**, *18*, 872.

(8) (a) *Collect Data Collection Software*; Nonius, B. V.; Delft, The Netherlands, 1998. (b) *HKL2000 and maXus Softwares*; University of Glasgow, Scotland, U.K.; Nonius, B. V.; Delft, The Netherlands; MacScience Co. Ltd.: Yokohama, Japan, 2000.

(9) (a) Blessing, R. H. *Acta Crystallogr.* **1995**, *A51*, 33. (b) Blessing, R. H. *J. Appl. Crystallogr.* **1997**, *30*, 421.

(10) Sheldrick, G. M. *SHELX 97, Program for the Solution of Crystal Structures Determination*; PC Version; University of Göttingen: Göttingen, Germany, 1997.

(11) Sheldrick, G. M. *SHELX 97, Program for the Refinement of Crystal Structures*; PC Version; University of Göttingen: Göttingen, Germany, 1997.

Table 1. Crystallographic Data for Compounds **2·Co**, **3·Ni**, **4·Mn**, and **5·Co**

	2·Co	**3·Ni**	**4·Mn**	**5·Co**
formula	$CoN_4H_{10}S_2O_8$	$NiN_4H_{10}S_2O_8$	$MnN_2H_4SO_4$	$CoN_2H_4SO_4$
fw	317.16	316.92	183.05	187.05
T, K	293	293	293	293
crystal system	triclinic	triclinic	orthorhombic	orthorhombic
space group	$P\bar{1}$	$P\bar{1}$	$Pccn$	$Pccn$
a, Å	5.2667(11)	5.2667(11)	6.4122(13)	6.3020(13)
b, Å	5.8284(12)	5.8284(12)	7.8799(16)	7.6219(15)
c, Å	7.3005(15)	7.3005(15)	9.0745(18)	8.8799(18)
α, deg	90.57(3)	90.57(3)	90	90
β, deg	105.73(3)	105.73(3)	90	90
γ, deg	98.93(3)	98.93(3)	90	90
V, Å^3	212.78(8)	212.78(8)	458.51(16)	426.53(15)
Z	2	2	4	4
D_c, g/cm^3	2.475	2.474	2.652	2.913
μ (Mo K_α), mm^{-1}	2.547	2.810	3.249	4.421
crystal size, mm^3	0.19 × 0.12 × 0.10	0.19 × 0.12 × 0.10	0.20 × 0.12 × 0.10	0.19 × 0.13 × 0.11
T_{min} and T_{max}	0.6433, 0.7848	0.6173, 0.7664	0.5627, 0.7371	0.528, 0.782
θ_{min}, θ_{max}, deg	3.54, 27.80	3.54, 27.47	4.10, 25.96	4.20, 27.46
R1 [a],wR2 [b] [$I \geq 2\sigma(I)$]	0.0279, 0.0833	0.0262, 0.0724	0.0273, 0.0740	0.0193, 0.0566
R1 [a],wR2[b] (all data)	0.0343, 0.0616	0.0329, 0.1004	0.0369, 0.0761	0.0235, 0.0582
GOF	1.289	1.262	1.040	1.075
$\Delta\rho$[c], e/Å^3	0.202, −0.236	0.221, −0.288	0.303, −0.372	0.256, −0.259
max. and mean[d] Δ/σ	0.000, 0.000	0.000, 0.000	0.000, 0.000	0.000, 0.000

[a] $R1 = \Sigma||F_o| - |F_c||/\Sigma|F_o|$. [b] $wR2 = |\Sigma w(|F_o|^2 - |F_c|^2)|/\Sigma|w(F_o)^2|^{1/2}$. [c] Maximum and minimum residual density. [d] Maximum and mean shift/sigma.

Elemental analysis of nitrogen, hydrogen, and sulfur was performed using an Elementar Vario EL analyzer. FTIR spectra were recorded against pure samples in the range of 4000−600 cm^{-1} using a Nicolet iN10 MX Microinfrared Spectrometer.

Magnetic measurements were performed using a Quantum Design MPMSXL5 SQUID system with samples tightly packed and sealed in a capsule. Diamagnetic corrections were estimated by using Pascal constants[12] and background corrections by experimental measurement on sample holders.

Theoretical Calculations. Density functional theory (DFT) calculations were performed using spin-unrestricted Kohn−Sham formalism with the hybrid B3LYP functional[13,14] as implemented in the Gaussian 09 program suite.[15] The 6-311G (*d*, *p*) basis set for Ni, Mn and the 6-31G(*d*, *p*) basis set for other light atoms were employed. The positions of the non-hydrogen atoms were taken from the structures of compounds **3·Ni** and **4·Mn**. The locations of hydrogen atoms were fully optimized at B3LYP/6-31G* level of theory.

Results and Discussion

Synthesis. Hydrothermal reactions have provided convenient and effective routes for the isolation of high-quality single crystals.[16,17] In this work, we adopt different reactant as hydrazine source. In the above synthesis process, in situ reactions are carried out through the decomposition of 3,4′-bitriazole (Btr) molecule (Detailed information depicted in Scheme 1 of the Supporting Information). The reaction temperature, the reaction time and the ratio of metal to ligand are all the important conditions to obtain these complexes. It was found that the higher reaction temperature, longer reaction time and higher ratio of metal to Btr resulted in higher quality and purer complexes in the method of in situ hydrothermal reaction. Furthermore it is of more possibility to get bigger crystals through in situ hydrothermal reaction. The addition of hydrofluoric acid protonates hydrazine molecule and results in the one-dimension compounds **1**−**3** in both in situ reactions and direct reactions.

IR Spectroscopy. The IR spectrum of compounds **1**−**6** reveal the presence of the hydrazine groups (N_2H_4) and the sulfate groups (SO_4^{2-}) (Figure S2 in the Supporting Information). The spectra can be divided roughly into four feature regions and some small differences can be found in 1D and 3D compounds because of different coordination modes of hydrazine and sulfate. For 1D compounds **1**−**3** with protonated hydrazine molecule as terminal ligand, the ν(N−N) band is at 988 cm^{-1}. For 3D compounds with hydrazine molecule as bridging ligand, the ν (N−N) band is at 967 cm^{-1} for **4·Mn**, 980 cm^{-1} for **5·Co**, and 989 cm^{-1} for **6·Ni**. It can be seen that the N−N stretching bands of hydrazine ligand are stronger than ν (N−N) = 885 cm^{-1} of the solid hydrazine, which is consistent with the previous report.[5,18,19] In the range of 1500−1650 cm^{-1}, N−H deformation vibration region, there are three consecutive bands in each of six complexes, but a strong band near 1500 cm^{-1} appears additionally in

(12) Mulay, L.N.; Boudreaux, E.A., *Theory and Applications of Molecular Diamagnetism*; Wiley: New York, 1976.
(13) Becke, A. D. *J. Chem. Phys.* **1993**, *98*, 5648.
(14) Lee, C.; Yang, W.; Parr, R. G. *Phys. Rev.* **1988**, *B37*, 785.
(15) Frisch, M. J.; Trucks, G. W.; Schlegel, H. B.; Scuseria, G. E.; Robb, M. A.; Cheeseman, J. R.; Scalmani, G.; Barone, V.; Mennucci, B.; Petersson, G. A.; Nakatsuji, H.; Caricato, M.; Li, X.; Hratchian, H. P.; Izmaylov, A. F.; Bloino, J.; Zheng, G.; Sonnenberg, J. L.; Hada, M.; Ehara, M.; Toyota, K.; Fukuda, R.; Hasegawa, J.; Ishida, M.; Nakajima, T.; Honda, Y.; Kitao, O.; Nakai, H.; Vreven, T.; Montgomery, J. A., Jr.; Peralta, J. E.; Ogliaro, F.; Bearpark, M.; Heyd, J. J.; Brothers, E.; Kudin, K. N.; Staroverov, V. N.; Kobayashi, R.; Normand, J.; Raghavachari, K.; Rendell, A.; Burant, J. C.; Iyengar, S. S.; Tomasi, J.; Cossi, M.; Rega, N.; Millam, J. M.; Klene, M.; Knox, J. E.; Cross, J. B.; Bakken, V.; Adamo, C.; Jaramillo, J.; Gomperts, R.; Stratmann, R. E.; Yazyev, O.; Austin, A. J.; Cammi, R.; Pomelli, C.; Ochterski, J. W.; Martin, R. L.; Morokuma, K.; Zakrzewski, V. G.; Voth, G. A.; Salvador, P.; Dannenberg, J. J.; Dapprich, S.; Daniels, A. D.; Farkas, O.; Foresman, J. B.; Ortiz, J. V.; Cioslowski, J.; Fox, D. J. *Gaussian 09*, revision A.1; Gaussian, Inc.: Wallingford, CT, 2009.
(16) (a) Feng, S.; Xu, R. *Acc. Chem. Res.* **2001**, *34*, 239–247. (b) Kim, K. *Chem. Soc. Rev.* **2002**, *31*, 96–107. (c) Salah, M. B.; Vilminot, S.; André, G.; Richard-Plouet, M.; Bourée-Vigeron, F.; Mhiri, T.; Kurmoo, M. *Chem.—Eur. J.* **2004**, *10*, 2048–2057.
(17) Zhang, X. M. *Coord. Chem. Rev.* **2005**, *249*, 1201–1219.
(18) Braibanti, A.; Dallavalle, F.; Pellinghelli, M. A.; Leporati, E. *Inorg. Chem.* **1968**, *7*, 1430–1433.
(19) (a) Duber, E.; Oswald, H. R. *Helv. Chim. Acta* **1971**, *54*, 1621–1628. (b) Duber, E.; Oswald, H. R. *Helv. Chim. Acta* **1971**, *54*, 1628–1637.

Table 2. Selected Bond Lengths (Å) and Bond Angles (deg) for Compounds **2·Co**, **3·Ni**, **4·Mn**, and **5·Co**[a]

	2·Co	**3·Ni**		**4·Mn**	**5·Co**
M(1)−O(2)	2.0995(18)	2.0782(16)	M(1)−O(1)	2.181(2)	2.1021(14)
M(1)−O(2)#1	2.0995(18)	2.0782(16)	M(1)−O(1)#4	2.181(2)	2.1021(14)
M(1)−O(4)#2	2.0984(19)	2.0980(18)	M(1)−O(2)#5	2.209(2)	2.1436(15)
M(1)−O(4)#3	2.0984(19)	2.0980(18)	M(1)−O(2)#6	2.209(2)	2.1436(15)
M(1)−N(1)	2.109(2)	2.077(2)	M(1)−N(1)	2.227(3)	2.1218(19)
M(1)−N(1)#1	2.109(2)	2.077(2)	M(1)−N(1)#4	2.227(3)	2.1218(19)
N(1)−N(2)	1.433(3)	1.441(3)	N(1)−N(1)#8	1.465(5)	1.464(4)
O(2)−S(1)	1.4844(17)	1.4922(16)	O(1)−S(1)	1.468(2)	1.4710(15)
O(3)−S(1)	1.4453(18)	1.4682(17)	O(1)#7−S(1)	1.468(2)	1.4710(15)
O(4)−S(1)	1.4655(18)	1.4720(18)	O(2)−S(1)	1.477(2)	1.4775(15)
O(5)−S(1)	1.4794(18)	1.4725(17)	O(2)#7−S(1)	1.477(2)	1.4775(15)
N(2)−N(1)−M(1)	116.27(16)	117.28(14)	N(1)#8−N(1)−M(1)	116.7(2)	118.98(18)
N(1)#1−M(1)−N(1)	180.000(1)	180.0	N(1)#4−M(1)−N(1)	180.00(17)	180.00(14)
O(2)#1−M(1)−O(2)	180.0	180.000(1)	O(1)#4−M(1)−O(1)	180.00(11)	180.00(8)
O(4)#2−M(1)−O(4)#3	180.0	180.0	O(2)#5−M(1)−O(2)#6	180.00(15)	180.00(5)
O(2)−M(1)−O(4)#3	92.94(7)	92.72(7)	O(1)−M(1)−O(2)#5	91.31(8)	92.33(6)
O(2)−M(1)−O(4)#2	87.06(7)	87.28(7)	O(1)−M(1)−O(2)#6	88.69(8)	87.67(6)
N(1)−M(1)−O(2)	87.23(8)	88.10(7)	N(1)−M(1)−O(1)	92.80(8)	95.19(6)
N(1)−M(1)−O(2)#1	92.77(8)	91.90(7)	N(1)−M(1)−O(1)#4	87.20(8)	84.81(6)
N(1)−M(1)−O(4)#3	94.52(9)	94.42(8)	N(1)−M(1)−O(2)#5	84.75(8)	84.34(6)
N(1)−M(1)−O(4)#2	85.48(9)	85.58(8)	N(1)−M(1)−O(2)#6	95.25(8)	95.66(6)
O−S1−O	108.27(10)−110.76(11)	107.41(10)−111.00(10)		108.66(11)−110.80(17)	108.43(8)−110.76(12)

[a] Symmetry transformations used to generate equivalent atoms: #1 $-x+1, -y, -z+2$; #2 $x+1, y, z$; #3 $-x, -y, -z+2$; #4 $-x, -y, -z$; #5 $x, -y+1/2, z-1/2$; #6 $-x, y-1/2, -z+1/2$; #7 $-x-1/2, -y+1/2, z$; #8 $-x+1/2, -y+1/2, z$.

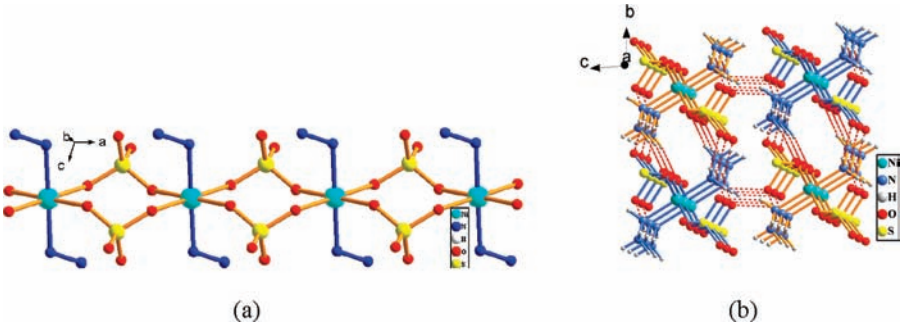

Figure 1. Structures of compounds 1−3, represented by **3·Ni.** (a) The 1D chain of $[M(SO_4)_2(N_2H_5)_2]_n$. Atomic scheme: M large turquiose spheres, N blue spheres, O red spheres, S yellow spheres. (b) The 3D H-bonding networks viewed down the $[M(SO_4)_2(N_2H_5)_2]_n$ chain direction.

the 1D compounds. This phenomenon is also due to the protonated hydrazine molecule as terminal ligand.

Crystal Structures. Crystallographic parameters for four compounds (**2·Co**, **3·Ni**, **4·Mn**, and **5·Co**) are listed in Table 1, selected bond lengths and angles in Table 2, and the data of H-bond in the Supporting Information

Compounds 1−3. Single-crystal X-ray structure determinations and powder X-ray diffraction (PXRD) analyses reveal that compounds **1−3** are isomorphous (Detailed information in the Experimental Section and Figure S1 in the Supporting Information) and crystallized in the triclinic space group $P\bar{1}$ (Table 1).

The structures of compounds **1−3** are composed of homometallic chains of $[M(SO_4)_2(N_2H_5)_2]_n$ (Figure 1). The octahedral M^{2+} ion is surrounded by four equatorial O atoms from four SO_4^{2-} anions and two axial N atoms from two terminal hydrazine molecules. The cis angles of O−M−O and the N−M−O are from 85.48° to 94.52° in **2·Co**, 85.58° to 94.42° in **3·Ni**, while all trans angles are 180.0° (Table 2).

Within the $[M(SO_4)_2(N_2H_5)_2]_n$ chains (Figure 1a), the adjacent M^{2+} ions are bridged by two O−S−O bridges of two SO_4^{2-} anions, with the unique M···M distance of 5.267 Å. The sulfate anion acts as an anti−anti bidentate mode to bridge the metal atoms. The infinite chain runs along *a* direction. The chains are further connected by hydrogen bonds into a 3D extended network, with the interchain M···M distances of 5.828, 7.301, 9.296 Å (Figure 1b). The H-bonds (N−H···O) is 2.742 Å for **2·Co** and 2.762 Å for **3·Ni** (Table 1 in the Supporting Information). The strong hydrogen bonding interactions between the chains are the crucial magnetic superexchange pathway to construct the 3D magnetic order in the 1D chain compounds, as will discuss later.

The hydrazine N_2H_4 is protonated to $N_2H_5^+$ and acts as a monodentate terminal ligand, which is rare in the unsubstituted hydrazine transition metal sulfates. Comparing with the reported complexes containing a monodentate hydrazine and the uncoordinated hydrazine (N−N = 1.460 Å), the distance between the two nitrogen atoms (1.432 Å for **2·Co**, 1.441 Å for **3·Ni**) is slightly shorter because of the protonation. This shortening can be probably attributed to diminution or suppression of the repulsion between the lone pairs.[5,20] Moreover the

(20) (a) Harmony, M. D.; Laurie, V. W. *J. Phys. Chem.* **1979**, *8*, 619. (b) Johnson, R. C. *Introductory Descriptive Chemistry*; W.A. Benjamin, Inc.: New York, 1966: p68.

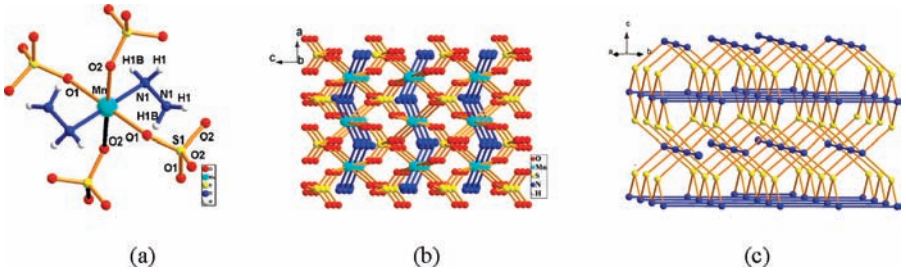

Figure 2. Structures of compounds **4**−**6**, represented by **4·Mn**. (a) The coordination environments of the metal ion and ligands. (b) Perspective view of the 3D framework structure of **4·Mn** along the *ac* direction. (c) Schematic view of the 3D network structure for **4·Mn**, sulfate (SO_4) reduced to S atom and H atom omitted.

angle of M−N−N (116.27° for **2·Co**, 117.28° for **3·Ni**) is also a little smaller than that of reported complexes.

Compounds 4−6. Single-crystal X-ray structure determinations and powder X-ray diffraction (PXRD) analyses also reveal that three compounds **4**−**6** are isomorphous (Detailed information in the Experimental Section and Figure S1 in the Supporting Information) and crystallized in the orthorhombic space group *Pccn* (Table 1). The main structures of these three compounds are the 3D neutral network involving M^{2+} ions connected by hydrazine N_2H_4 and sulfate anions SO_4^{2-} bridges (Figure 2). As shown in Figure 2a, represented by compound **4·Mn**, each M^{2+} ion resides at an inversion center and is six-coordinated in a distorted octahedral configuration, which includes two axial N atoms from two hydrazine bridges and four equatorial O atoms from four different SO_4^{2-} anions. The cis angles of O−M−O and the N−M−O are from 84.74° to 95.26° in **4·Mn**, 84.34° to 95.66° in **5·Co,** and all trans angles are 180° (Table 2). The N−N bond distance (1.465(5) Å for **4·Mn**, 1.464(4) Å for **5·Co**) and the angle of M−N−N (116.7° for **4·Mn**, 118.98° for **5·Co**) in the hydrazine bridging ligand are similar to the former ones.[5,21] Different from **1**−**3**, the structures of **4**−**6** can be regarded as the hydrazine bridged 1D chain M−N_2H_4−M which are connected into 3D framework by sulfate anions (Figure 2b, 2c and Figure S3 in the Supporting Information). The hydrazine molecules act as a trans bidentate bridging ligands and link the adjacent M^{2+} metal ions into the 1D infinite chains, with the M···M distance 5.08 Å. all these 1D chains are parallel to the *ab* plane, and run along two directions alternately: the $a + b$ direction and $a - b$ direction. The bridging SO_4^{2-} anions are above and below the layer alternatively. Hence every SO_4^{2-} anion links two chains with $a + b$ direction and another two with $a - b$ direction. Every 1D chain is connected further with four other chains by four SO_4^{2-} anions to generate a 3D structure.

In the above 3D structures, each M^{2+} metal ion is linked to twelve M^{2+} neighbors by hydrazine and sulfate bridges (Figure S3 in the Supporting Information). There are three kinds of the intranetwork M−M separations. One is the M−M separations through hydrazine bridges, 5.08 Å. The other two M−M separations are through sulfate bridges, 5.56 Å and 6.01 Å respectively. Thus, three magnetic coupling constants must be considered to interpret the magnetic properties of 3D compounds, which will be discussed in the section of Magnetostructural Correlations.

Although only hydrazine and sulfate ligands are contained in these 1D and 3D compounds, the versatile coordination and connection modes produce the diversified structures with various local and high dimensional symmetry, which is also one of the sources of magnetic-property difference shown below.

Magnetic Properties. Magnetic measurements were carried out on crystalline samples of compounds **1**−**6**. According to the magnetic data, it was suggested dominant antiferromagnetic coupling interactions between the M^{2+} ions in all six compounds. However, they exhibited various magnetic behaviors at low temperature and will be discussed in the following part by the sequence of the 1D compounds and 3D compounds, respectively.

Compounds 1−3. The magnetic properties of the three 1D compounds are similar due to their isomorphic structures. At room temperature, the $\chi_M T$ values of 4.40 (**1·Mn**), 2.94 (**2·Co**) and 1.30 $cm^3\ mol^{-1}$ K (**3·Ni**) are as expected for the isolated divalent metal ions.[22] The magnetic susceptibilities χ_M for compounds **1**−**3** in a field of 1kOe show a sharp peak upon cooling and reaches a maximum value of 0.247 $cm^3\ mol^{-1}$ at 5.0 K for **1·Mn,** 0.0997 $cm^3\ mol^{-1}$ at 7.0 K for **2·Co** and 0.0469 $cm^3\ mol^{-1}$ at 10.0 K for **3·Ni**, suggesting the presence of possible antiferromagnetic ordering in these three compounds (Figure 3). The magnetic susceptibility data in the range of 20−300K obey the Curie−Weiss law, $\chi_M = C/(T - \theta)$, with Curie constant C = 4.59 (**1·Mn**), 3.17 (**2·Co**) and 1.35 $cm^3\ mol^{-1}$ K (**3·Ni**), negative Weiss constants θ of −10.3 K (**1·Mn**), −22.4 K (**2·Co**) and −12.5 K (**3·Ni**). The Neel temperature, T_N, was determined from the sharp peak of $d(\chi_M T)/dT$ at 4.5 K for **2·Co** and **3·Ni** but there is no sharp peak of $d(\chi_M T)/dT$ for **1·Mn** (Inset of Figure 3a).[23] The ratios of $T_N/T(\chi_{M,max})$ = 0.643 for **2·Co** and 0.45 for **3·Ni** do show the low-dimensional antiferromagnetic ordering character.[24] The field dependence of the magnetization of **1**−**3** measured at 2 K increase linearly (Figure 3c). At 2 K, the magnetization at 50 kOe is only 2.66 Nβ for **1·Mn**, 0.98 Nβ for **2·Co**, and

(21) (a) Barrado, G.; Miguel, D.; Riera, V.; Garcia-Granda, S. *J. Organomet. Chem.* **1992**, *489*, 129. (b) Mosier, P. E.; Kim, C. G.; Coucouvanis, D. *Inorg. Chem.* **1993**, *32*, 2620. (c) Sellmann, D.; Kreutzer, P.; Huttner, G.; Frank, A. *Z. Naturforsch. B* **1978**, *33*, 1341.

(22) Bourdreaux, E. A.; Mulay, L. N. *Theory and Application of Molecular Magnetism*; Wiley: New York, 1976.

(23) (a) Fisher, M. E. *Proc. R. Soc. London, Ser. A* **1960**, *254*, 66–85. (b) Fisher, M. E. *Philos. Mag.* **1962**, *7*, 1731. (c) Tian, Y. Q.; Cai, C. X.; Ren, X. M.; Duan, C. Y.; Xu, Y.; Gao, S.; You, X. Z. *Chem.—Eur. J.* **2003**, *9*, 5673–5685.

(24) DeFotis, G. C.; Remy, E. D.; Scherrer, C. W. *Phys. Rev. B* **1990**, *41*, 9074.

0.27 Nβ for **3·Ni,** far from the saturation values of ~5, 3, and 2 Nβ expected for one isolated spin $S = 5/2$, 3/2, and 1, respectively. This is another evidence supporting antiferromagnetic ordering in the 1D compounds.

Considering the 1D equally spaced chain structures, the $\chi_M T$ value of **1·Mn and 2·Co** can be fitted by Fisher's 1D Heisenberg chain model[25−27] ($S = 5/2$ and $S = 3/2$, $H = -2JS_iS_j$) expressed by the following equation:

$$\chi_{\text{chain}} = \frac{Ng^2\beta^2 S(S+1)}{3kT}\frac{1+u}{1-u} \qquad (1)$$

where

$$u = \coth\left[\frac{2JS(S+1)}{kT}\right] - \left[\frac{kT}{2JS(S+1)}\right]$$

J is the coupling constant of the neighboring M^{2+} bridged by SO_4^{2-}. N, g, β, k, and T have their usual meanings. The interchain interaction term zj' at the mean field approximation is added to describe the interchains spin−spin interactions.[28,29] Thus the expression for the magnetic susceptibility becomes

$$\chi_{\text{M}} = \frac{\chi_{\text{chain}}}{1-(2zj'/Ng^2\beta^2)\chi_{\text{chain}}} \qquad (2)$$

The $\chi_M T$ value of **3·Ni** also can be fitted with the following analytical expression for an antiferromagnetic chain of $S = 1$ with the Hamiltonian $H = -2JS_iS_j$. The interchain interaction (zj') is also added in terms of mean field theory.[25,30]

$$\chi_{\text{chain}} = \frac{Ng^2\beta^2}{kT}\frac{2.0+0.0194x+0.777x^2}{3.0+4.346x+3.232x^2+5.834x^3} \qquad (3)$$

where $x = |2J|/kT$. J is the coupling constant of the neighboring Ni^{2+} bridged by SO_4^{2-}. N, g, β, k, and T have their usual meanings.

The best fitting parameters are $J = -0.52$ cm^{-1}, $zj' = -0.28$ cm^{-1}, $g = 2.04$, and $R = 3.6 \times 10^{-3}$ for **1·Mn** (R is defined as $\Sigma[(\chi_M T)_{\text{obs}} - (\chi_M T)_{\text{calcd}}]^2/\Sigma[(\chi_M T)_{\text{obs}}]^2$). For **2·Co**, the corresponding fitting parameters are $J = -2.42$ cm^{-1}, $zj' = -0.32$ cm^{-1}, $g = 2.69$, and $R = 3.2 \times 10^{-4}$. For **3·Ni**, the best fitting gives $J = -2.52$ cm^{-1}, $zj' = -0.34$ cm^{-1}, g = 2.32, and $R = 1.08 \times 10^{-4}$.

Seen from magnetic data of the above three 1D compounds, it is clear that AF coupling occurs not only between intrachain metal ions but also interchain metal centers. The interchain AF coupling is transmitted by hydrogen bonds which should be responsible for the occurrence of long-range ordering. Obviously the antiferromagnetic coupling between intrachain metal ions is transmited by the sulfate bridge but terminal hydrazine ligand just plays the role in the interchain coupling through the hydrogen bonds.

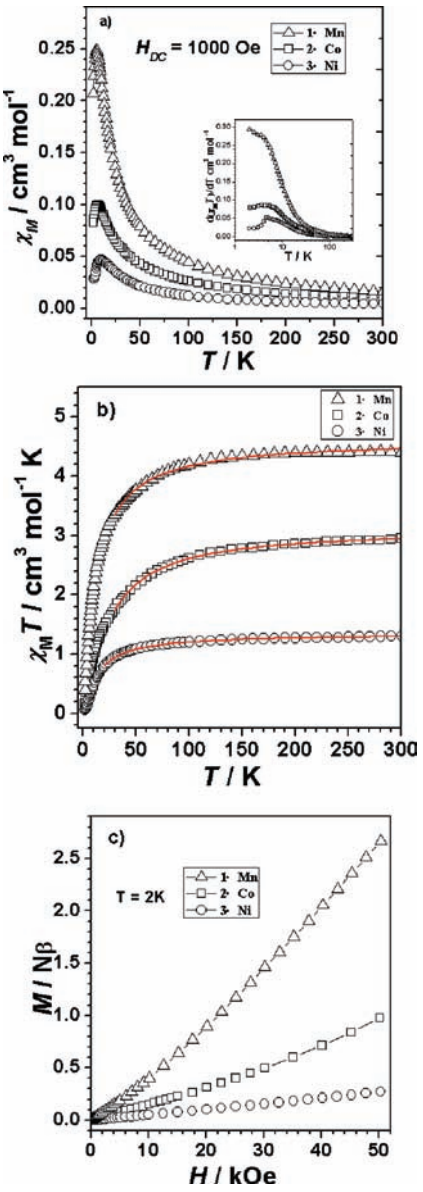

Figure 3. (a) Plots of temperature dependence of χ_M and $d(\chi_M T)/dT$ of compounds **1**−**3** measured at a 1kOe field. (b) plot of temperature dependence of $\chi_M T$ under a 1kOe field. The red line shows the best fit obtained by using a 1D Fisher model. (c) Magnetization versus applied magnetic field at 2.0K for compounds **1**−**3**.

Compounds 4−**6.** For the 3D compounds, hydrazine as bridging ligand is expected to transmit the stronger magnetic coupling between M^{2+} ions than that in 1D compounds. Although the 3D compounds **4**−**6** are also isomorphous, their magnetic properties are quite different, especially at the low temperature region owing to the different spin paramagnetic centers, isotropic Mn^{2+} and anisotropic Co^{2+}, Ni^{2+}. The various magnetic behaviors of **4**−**6** are discussed in details below.

4·Mn. The temperature variable magnetic susceptibility of **4·Mn** was measured in the range of 2−300 K under 1 kOe applied field (Figure 4). At 300K, $\chi_M T$ is 4.30 cm^3 mol^{-1} K, close to the expected spin-only value of

(25) Kahn, O. *Molecular Magnetism*; VCH: New York, 1993.
(26) Fisher, M. E. *Am. J. Phys.* **1964**, *32*, 343.
(27) (a) Liu, T. F.; Fu, D.; Gao, S. *J. Am. Chem. Soc.* **2003**, *125*, 13976. (b) Sun, H. L.; Wang, Z. M.; Gao, S. *Chem.—Eur. J.* **2009**, *15*, 1757–1764.
(28) (a) Myers, B. E.; Berger, L.; Friedberg, S. *J. Appl. Phys.* **1969**, *40*, 1149. (b) O'Connor, C. J. *Prog. Inorg. Chem.* **1982**, *29*, 203.
(29) (a) Carlin, R. L. *Magnetochemistry*; Springer: Heidelberg, Germany, 1986. (b) Carlin, R. L.; van Duyneveldt, A. J. *Magnetic properties of Transition Metal Compounds*; Springer: New York, 1977.
(30) Weng, C. Y. Ph.D. Thesis, Carnegie Institute of Technology: Pittsburgh, PA, 1968.

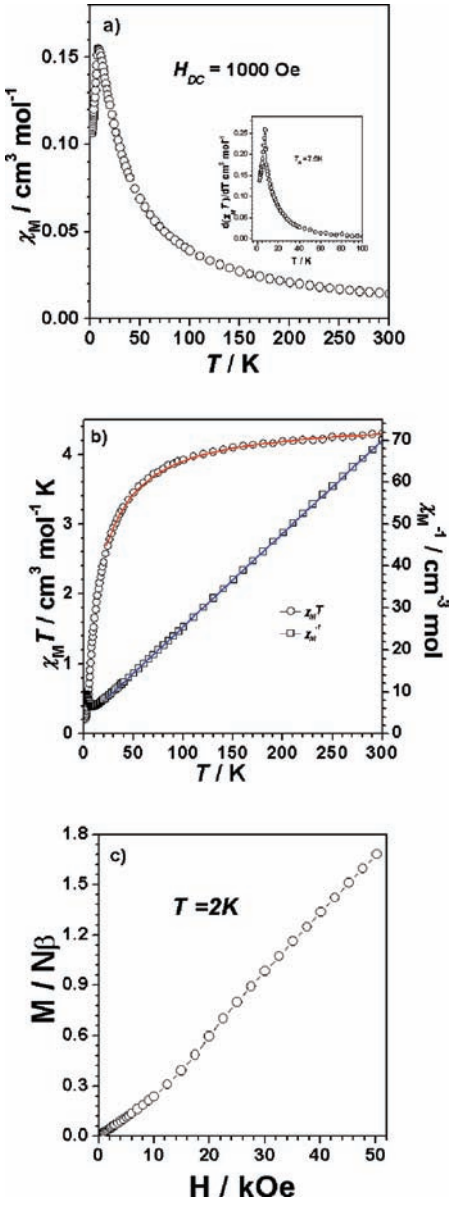

Figure 4. (a) Plots of temperature dependence of χ_M and $d(\chi_M T)/dT$ of **4·Mn** measured at a 1kOe field. (b) Plot of temperature dependence of $\chi_M T$ and χ_M^{-1} under a 1kOe field. The red line shows the best fit obtained by using a 3D HTSE model, and the blue line represents the best fit to the Curie−Weiss law. (c) Magnetization versus applied magnetic field at 2.0K for **4·Mn**.

4.37 cm^3 mol^{-1} K for Mn^{2+} ions with $S = 5/2$. The magnetic data above 30 K can be fitted by Curie−Weiss law with the Curie constant $C = 4.50$ cm^3 mol^{-1} K and the negative Weiss constant $\theta = -15.3$ K, which indicates the antiferromagnetic interaction between Mn^{2+} ions. The magnetic susceptibility χ_M increases upon cooling, reaches a maximum of 0.155 cm^3 mol^{-1} at 8.0 K and then sharply goes down to the value of 0.106 cm^3 mol^{-1} at 2.0 K. This value is account for about 2/3 of the maximum χ_M value of 0.155 cm^3 mol^{-1}, which is the typical character of a 3D antiferromagnet. The Neel temperature, T_N, was determined from the peak of $d(\chi_M T)/dT$ at 7.5 K (inset of Figure 4a). For 3D Heisenberg antiferromagnet the ordering temperature is very close to $T(\chi_{M,\,max})$.[24,31] So the ratio of $T_N/T(\chi_{M,max}) = 0.938$ for **4·Mn** is consistent with the prediction of the three-dimensional antiferromagnetic ordering. The field dependence of the magnetization of **4·Mn** measured at 2 K increase nearly linearly at field range 0−9 kOe, and after an abnormality at about 9−10 kOe, it increases up to 50 kOe and reaches 1.68 $N\beta$, far from the saturation values of ~5 Nβ for a spin-only Mn^{2+} ion. (Figure 4c). The $M(T,H)$ behavior is typical for an antiferromagnet, and the slight abnormality of magnetization at 9−10kOe indicates that a spin-flop transition occurs, as can be found in many antiferromagnets with weak anisotropy (e.g., Mn^{2+}).[28]

On the basis of the structural analysis, χ_M of **4·Mn** in the high-temperature region may be fitted by the HTSE model developed by Rushbook and Wood.[32] For Heisenberg antiferromagnet ($S = 5/2$) of the face-centered cubic network (z = 12) with the Hamiltonian $H = -2J\Sigma_{ij}S_i \cdot S_j - g\beta H\Sigma_i S_{3i}$, the expression for the magnetic susceptibility becomes

$$\chi = \frac{Ng^2\beta^2 S(S+1)}{3kT}\left(1+\sum_{n=1}^{6} C_n x^n\right)^{-1} \qquad (4)$$

with $x = J/kT$, and $C_1 = -70$, $C_2 = 443.33$, $C_3 = 8\,855.78$, $C_4 = 231548.01$, $C_5 = 7\,030166.54$, $C_6 = 7\,030166.54$. N, J, g, β, S, k, and T have their usual meanings. The best fitting of the data above 30 K gives $J = -0.15$ cm^{-1}, $g = 2.03$, and $R = 1.08 \times 10^{-4}$.

At the same time, according to the molecular field theory of antiferromagnetism, the Weiss temperature can be expressed as[25,33]

$$\theta = 2S(S+1)zJ/3k \qquad (5)$$

where z is the magnetic coordination number of a lattice site. For **4·Mn**, it is deduced that $\theta = -15.3$ K, S = 5/2, $z = 12$, and $J = -0.15$ cm^{-1}, which are consistent well with the results of the HTSE model.

5·Co. The temperature dependence of the magnetic susceptibility of **5·Co** was measured in a field of 1 kOe from 2 to 300 K (Figure 5). The room-temperature $\chi_M T$ value of 3.07 cm^3 mol^{-1} K is significantly larger than the expected spin-only value of 1.875 cm^3 mol^{-1} K for $S = 3/2$, which is close to the experimental values reported for other Co^{2+} compounds.[21,34] The $\chi_M T$ versus T plot shows that $\chi_M T$ decreases continuously upon cooling and reaches a minimum value of 0.56 cm^3 mol^{-1} K at 5 K. Then it increases to a maximum of 1.873 cm^3 mol^{-1} K at 2.5 K, followed by a rapidly drop toward zero. The upturn of $\chi_M T$ below 5 K suggests a possible magnetic phase transition. The fitting of the χ_M data from 10 to 300 K with the Curie−Weiss law gives a Curie constant

(31) Puertolas, A.; Navarro, R.; Palacio, F.; Bartolome, J.; Gonzalez, D.; Carlin, R. L. *Phys. Rev. B* **1982**, *26*, 395.

(32) Rushbrook, G. S.; Wood, P. J. *Mol. Phys.* **1958**, *1*, 257–283.

(33) (a) De Jongh, L. J.; Miedema, A. R. *Adv. Phys.* **1974**, *23*, 947–1170. (b) Coronado, E.; Delhaes, P.; Gatteschi, D.; Miller, J. S. *Molecular Magnetism: From Molecular Assemblies to the Device*; NATO ASI Series; NATO: Washington, DC, 1995. (c) Miller, J. S.; Drillon, M. *Magnetism: Molecules to Materials*; Wiley-VCH: Weinheim, Germany, 2002−2005, Vol. *I*−*V*.

(34) (a) Wang, X. Y.; Wei, H. Y.; Wang, Z. M.; Chen, Z. D.; Gao, S. *Inorg. Chem.* **2005**, *44*, 572–583. (b) Sun, H. L.; Wang, Z. M.; Gao, S. *Inorg. Chem.* **2005**, *44*, 2169–2176. (c) Yang, B. P.; Prosvirin, A. V.; Guo, Y. Q.; Mao, J. G. *Inorg. Chem.* **2008**, *47*, 1453–1459.

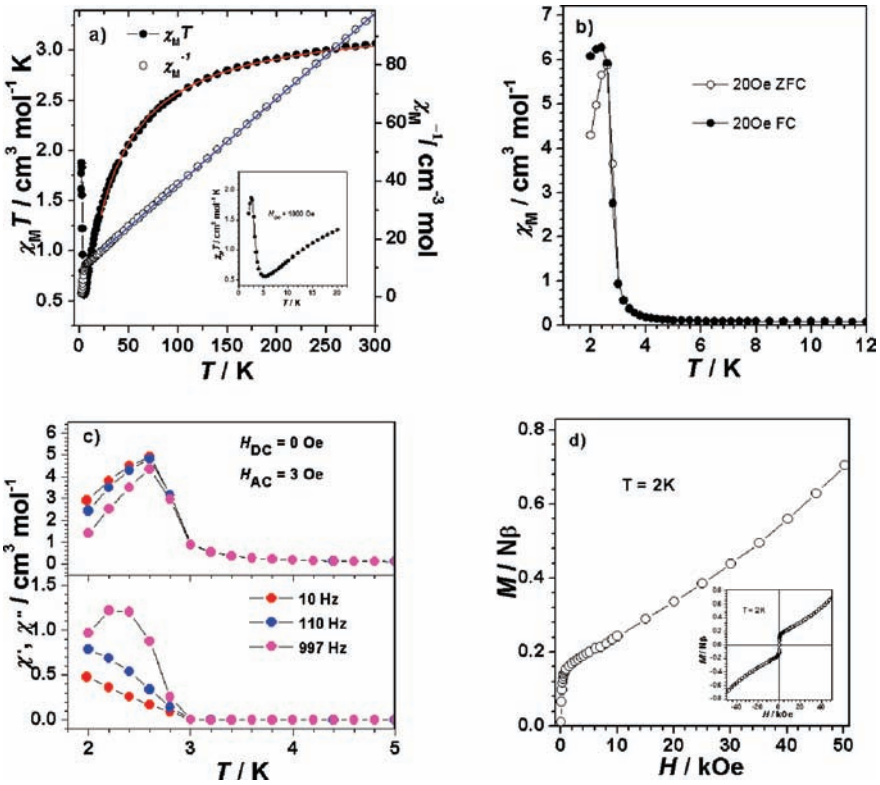

Figure 5. (a) Plot of temperature dependence of $\chi_M T$ and $\chi_M{}^{-1}$ under a 1kOe field for **5·Co**. The red line shows the best fit obtained by using a 3D HTSE model, and the blue line represents the best fit to the Curie−Weiss law. Inset: the enlargement of the low temperature χ_MT. (b) ZFCM and FCM of **5·Co** at external field of 20 Oe. (c) Plots of temperature dependence of AC susceptibility χ_M' (top) and χ_M'' (down) in zero applied dc field and an ac field of 3 Oe at different frequencies (10,110,997 Hz). (d) Magnetization versus applied magnetic field at 2.0K. Inset: Hysteresis loop at 2 K.

C = 3.39 cm^3 mol^{-1} K and a negative Weiss constant θ of −32.3 K. The high value of C (1.875 cm^3 mol^{-1} K for spin-only Co^{2+}) and the big negative Weiss constant may be partly contributed by the strong spin−orbit coupling, which is remarkable for the $^4T_{1\ g}$ state of Co^{2+} in an octahedral ligand field. The big negative Weiss constant θ may also indicates the coexistence of antiferromagnetic interactions between adjacent Co^{2+} ions.

The increase in $\chi_M T$ observed at low temperature might correspond to the onset of a weak ferromagnetic state because of spin canting of the antiferromagnetically coupled Co^{2+} ions. Long range magnetic ordering is clearly evident from low-field magnetization and ac susceptibility measurements. Both the temperature dependence of the zero-field-cooled magnetization and the temperature dependence of the field-cooled magnetization (ZFCM and FCM) measured in a low field of 20 Oe show a divergence at ∼2.5 K (Figure 5b).This behavior is consistent with a spontaneous magnetization under a long-range magnetic phase transition. Moreover, the peak in the in-phase component χ_M' of the *ac* susceptibility at 2.5 K is in agreement with above ZFCM/FCM results (Figure 5c). The nonzero out-of-phase component χ_M'' supports a ferromagnetic nature of the transition. Additionally, frequency dependence of out-of-phase component χ_M'' is observed, which can be attributed to the movement of the domain wall for this weak ferromagnet with spontaneous magnetization.[35] The field dependence of the magnetization, $M(H)$ at 2 K shows an abrupt increase at fields below 500 Oe and a steady increase to 0.705 Nβ at 50 kOe without achieving saturation (Figure 5d). Examining carefully the data in the low-field region, no detected hysteresis loop is observed at 2 K. Therefore, **5·Co** is regarded as a 3D weak ferromagnet due to spin-canting with the critical temperature 2.5K. According to the 3D structural feature of **5·Co**, the lack of centrosymmetry between the neighboring Co^{2+} ions bridged by hydrazine and sulfate ligands, allows the occurrence of Dzyaloshinsky−Moriya (DM) interaction or antisymmetric exchange interaction.[36] Moreover, the single-ion anisotropy of Co^{2+} enhances this interaction because the antisymmetric exchange is proportional to the single-ion anisotropy. The combination of single-ion and structural anisotropies competes with overall AF interaction and results in spin-canted weak ferromagnetism.

For high-spin octahedral Co^{2+} (d^7, S = 3/2), the ground state $^4T_{1g}$ is always difficult to be magnetically analyzed because of unquenched orbital contribution and spin−orbit coupling. Recently some efforts have been made to calculate the spin−orbit coupling parameter λ (λ = −170 cm^{-1} for free ion), the axial splitting parameter Δ and the axial zero-field splitting parameter D.[37,38] In the case of **5·Co**, we try to analyze the susceptibility

(35) Balanda, M. In *Relaxation Phenomena: Liquid Crystal, Magnetic Systems, Polymers High-Tc Superconductors, Metallic Glass*; Haase, W., Wróbel, S., Eds.; Springer: Berlin, Germany, 2003; pp 97−99.

(36) (a) Dzyaloshinsky, I. *J. Phys. Chem. Solids* **1958**, *4*, 241. (b) Moriya, T. *Phys. Rev.* **1960**, 120,91.

(37) Mabbs, F. E.; Machin, D. J. *Magnetism and Transition Metal Complexes*; Chapman and Hall: London, 1973.

(38) Figgis, B. N.; Gerloch, M.; Lewis, J.; Mabbs, F. E.; Webb, G. A. *J. Chem. Soc. A* **1968**, 2086–2093 and references therein.

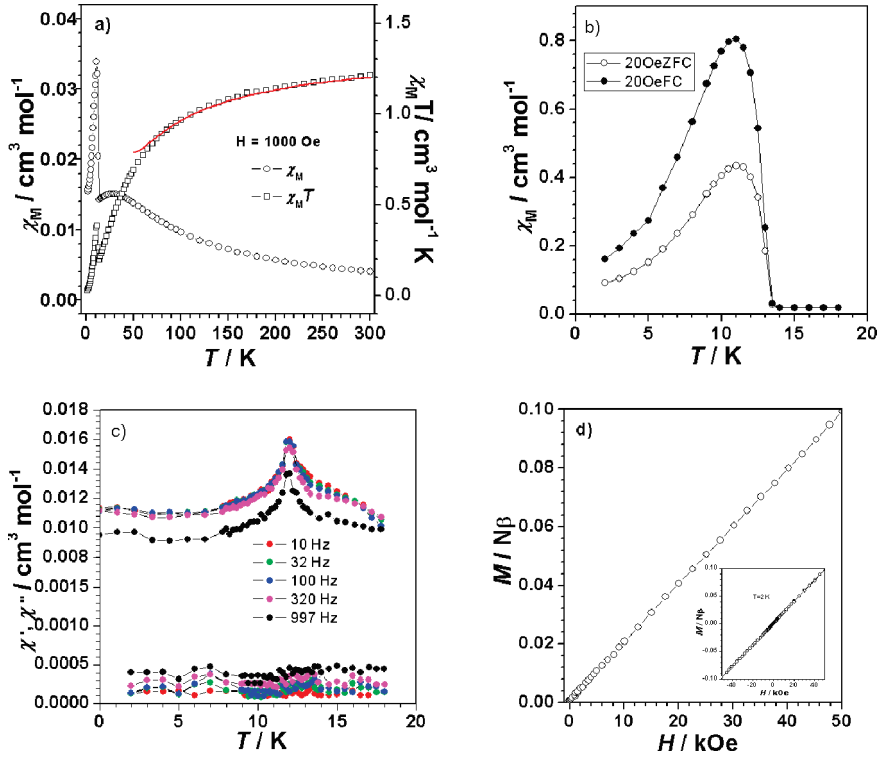

Figure 6. (a) plot of temperature dependence of $\chi_M T$ and χ_M under a 1kOe field for **6·Ni**. The red line shows the best fit obtained by using a 3D HTSE model. (b) ZFCM and FCM of **6·Ni** at external field of 20 Oe. (c) Plots of temperature dependence of AC susceptibility χ_M' (top) and χ_M'' (down) in zero applied dc field and an ac field of 3 Oe at different frequencies (10, 32, 100, 320, and 997 Hz) .(d) Magnetization versus applied magnetic field at 2.0K. Inset: Hysteresis loop at 2 K.

data by using a mononuclear Co^{2+} with spin−orbit coupling at the molecular-field approximation. The Hamiltonian for spin−orbit coupling is written as $H = -\lambda LS$. The χ_{mono} for a mononuclear Co^{2+} complex in an octahedral environment can be calculated from the following equation[37]

$$\chi_{mono} = \frac{1}{T}\left[\frac{7(3-A)^2x}{5}+\frac{12(2+A)^2}{25A} + \left(\frac{2(11-2A)^2x}{45}+\frac{176(2+A)^2}{675A}\right)\exp\left(\frac{-5Ax}{2}\right) + \left(\frac{(5+A)^2x}{9}-\frac{20(2+A)^2}{27A}\right)\exp(-4Ax)\right] / \frac{8x}{3}\left[3+2\exp\left(\frac{-5Ax}{2}\right)+\exp(-4Ax)\right] \quad (6)$$

where $x = \lambda/kT$, A is a scaling factor of the crystal-field strength relative to the interelectronic repulsions (1.5 for a weak field, 1.0 for a strong field, and 1.32 for a free ion). Due to the magnetic interaction between paramagnetic ions, the expression of susceptibility in eq 6 is corrected using the molecular field approximation (eq 7). where χ is the experimental exchange-coupled magnetic susceptibility and zJ is the total exchange parameter between Co^{2+} ions, the other symbols have their usual meanings.[34]

$$\chi = \frac{T\chi_{mono}}{T-\theta} \quad (7)$$

where

$$\theta = \frac{2zJS(S+1)}{3k}$$

The magnetic data were fitted in the temperature range of 20−300 K gives $\lambda = -108\ cm^{-1}$ and $A = 1.21$. It should be taken into account the term $\lambda = k\lambda_{freeion}$,[37] where k is a reduction factor of spin−orbit coupling because of covalency ($k = 0.635$). The negative value of $J = -0.74\ cm^{-1}$ indicates that the magnetic coupling between Co^{2+} ions is antiferromagnetic, which is mediated by hydrazine and sulfate molecules.

Considering the 3D crystal structure, the magnetic susceptibility can be alternatively interpreted through the HTSE model as **4·Mn.** According to Co^{2+} ion with $S = 3/2$, the coefficients C_n in eq 4. are $C_1 = -30$, $C_2 = 90$, $C_3 = 722$, $C_4 = 7448.75$, $C_5 = 90595.45$, and $C_6 = 1202049.75$, respectively. The fitting results from the magnetic data above 30 K are $J = -0.71\ cm^{-1}$, $g = 2.68$ with $R = 1.08 \times 10^{-4}$. It can be seen that the results deduced from different model are comparable and the theory calculations agree well with the experimental data.

6·Ni. The temperature-dependent susceptibility of **6·Ni** in 2−300 K under an applied field of 1kOe is shown in Figure 6. After reaching a broad maximum ($\chi_{M,max} = 0.015\ cm^3\ mol^{-1}$) at ~28 K, the χ_M decreases slightly with decreasing temperature until 14 K, then increases abruptly to a peak at about 11 K, and decreases again to 2 K. The sharp peak indicates the occurrence of a long-range ordering below 14K, which may be caused by the

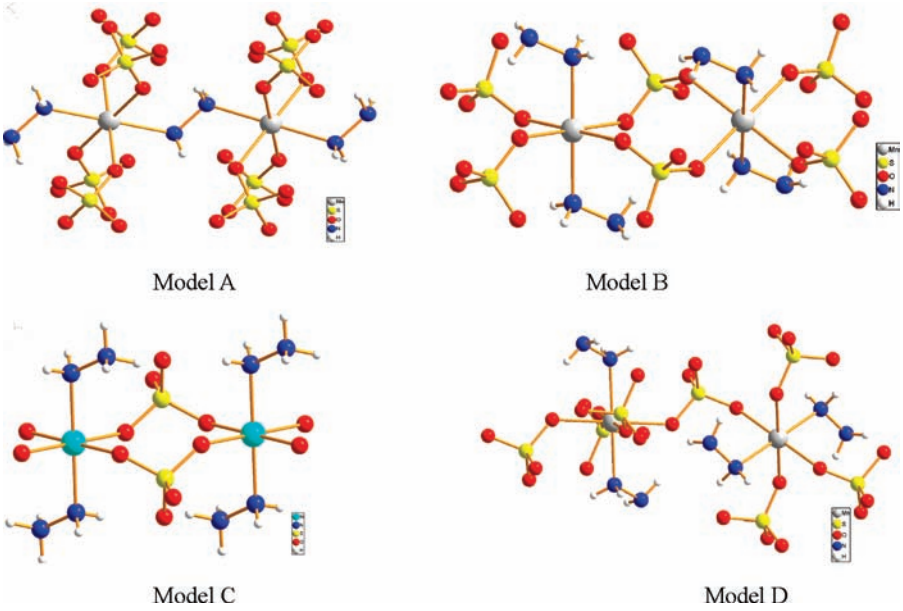

Figure 7. Model of the dimer units structures used for DFT calculation.

spin-canting. The $\chi_M T$ value decreases gradually from the room temperature value of 1.21 $cm^3\ mol^{-1}$ K, higher than the spin-only value 1.00 $cm^3\ mol^{-1}$ K for Ni^{2+} of $S = 1$, to a minimum at 14 K, and then increases to a peak at 12K with a further decrease until 2 K (Figure 6a). Fitting of the data above 30K with the Curie−Weiss law gives Curie constant $C = 1.4\ cm^3\ mol^{-1}$ K and a negative Weiss constant θ of −46.9 K, indicating antiferromagnetic interactions between adjacent Ni^{2+} ions.

To further clarify the nature of the low temperature phase, we measured the isothermal magnetization $M(H)$ at 2 K with field up to 50 kOe (Figure 6d). The magnetization increases almost linearly up to 50 kOe, and reaches 0.1 Nβ, far from the saturation value of 2 Nβ that is expected for one spin $S = 1$. The $M(H)$ behavior is typical for an antiferromagnet. Moreover hysteresis loop is not detected in the low-field region at 2 K.

The ZFCM/FCM and the ac susceptibility under $H_{dc} =$ 0 Oe, $H_{ac} =$ 3 Oe with frequencies of 10, 32, 110, 320, and 997 Hz from 2 to 18 K were measured. The ZFCM/FCM increases abruptly, and the in-phase signal of ac shows a sharp peak at ∼12.8 K (Figure 6b, c). This behavior indicates a spontaneous magnetization below 12.8 K. Although the magnetic phase transition arising from spin-canting is observed, the absence of the $\chi_M''(T)$ component suggests that **6·Ni** may be a hidden spin-canted weak ferromagnet. This weak ferromagnetism from canting may be hidden when many sublattices are present, such as in the system with hidden canting.[28,39]

For **6·Ni**, we can also treat the magnetic data with eq 4, the coefficients C_n for Ni^{2+}, S = 1, are $C_1 = -30$, $C_2 =$ 90, $C_3 = 722$, $C_4 = 7448.75$, $C_5 = 90595.45$, and $C_6 =$ 1202049.75, respectively. The fitting results from the magnetic data above 30 K are $J = -1.92\ cm^{-1}$, $g =$ 2.37 with $R = 3.87 \times 10^{-4}$.

Magnetostructural Correlations. To arrive at the better understanding of the magnetic behavior and getting insight into the magnetic exchange mechanism through the ligands hydrazine (N_2H_4) and sulfate (SO_4^{2-}) theoretically, quantum chemical density functional theory (DFT) calculations combined with the broken symmetry approach (DFT-BS), were performed. In the calculations, the geometry structures of the model complexes adapted the experimental crystal structure data. The details of the calculation method were described elsewhere.[40,41] Herein, our emphasis will be lie on the nature of the magnetic coupling interaction between the paramagnetic ions. For simplicity, we calculated only the model structures of the dimer units, where the bridge ligand SO_4^{2-} or N_2H_4 mediated the magnetic coupling of two paramagnetic ions (Figure 7). In the model A simplified from **4·Mn**, the N_2H_4 ligand linked two Mn^{2+} ions as two-atom bridge, but acted as terminal ligand in the model structure B, C, D simplified from **4·Mn**, **3·Ni**, and **4·Mn**, respectively. Correspondingly, the coordination bridges of the model B, C, D are single or double SO_4^{2-} groups.

On the basis of DFT-BS method, the relative magnitude of the magnetic coupling interactions for the above model structures was calculated. The three calculated magnetic coupling constant J for the hydrazine(N_2H_4) bridged model structure A and the other two sulfate bridged model structures B and D simplified from the 3D compound **4·Mn** are −1.37, −0.14, and −0.13 cm^{-1}, respectively, as compared to the total experimental fitting J value of $-0.15\ cm^{-1}$. At the same time, the calculated J value for the sulfate bridged model structure C of **3·Ni** are $-3.16\ cm^{-1}$ comparing with the experimental fitting J value of $-5.04\ cm^{-1}$. Both the calculated and the experimental fitting J values indicate consistently that the antiferromagnetic coupling between transition metal ions occurs through hydrazine (N_2H_4) and sulfate (SO_4^{2-}) bridging ligands. According to Oliver Kahn model, these

(39) Engelfriet, D. W.; Groeneveld, W. L.; Groenendijk, H. A.; Smit, J. J.; Nap, G. M. *Z. Naturforsch.* **1980**, *35a*, 115–128.

(40) Li, R. Y.; Wang, B. W.; Wang, X. T.; Gao, S. *Inorg. Chem.* **2009**, *48*, 7174–7180.

(41) Wang, B. W.; Wei, H. Y.; Wang, M. W.; Chen, Z. D. *J. Chem. Phys.* **2005**, *122*, 204310.

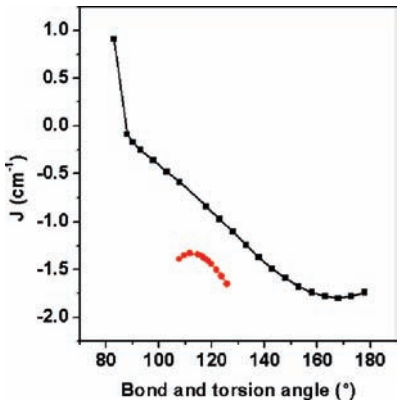

Figure 8. Plot of magnetic coupling constants calculated with DFT+BS method as a function of the variation of the bond and torsion angles for hydrazine bridge in **4·Mn**. Squares for *J* vs bond angle (Mn−N−N) and circles for *J* vs torsion angle (Mn−N−N−Mn).

results can be easily explained by the overlap of the magnetic orbital. For the high spin $3d^5$ electronic configuration of Mn^{2+} ion in octahedral environment, the dominant part of the magnetic couplings are the antiferromagnetic interactions between spin electrons with the same t_{2g} or e_g orbital symmetry. The intensity will be changed with the overlap of t_{2g} orbital or e_g orbitals of Mn^{2+} ions, in other words, changed with the torsion angle of two axis (N−Mn−Mn−N or Mn−N−N−Mn when hydrazine coordinating as terminal or bridging ligand) of coordinated Mn^{2+} centered octahedron. The torsion angles, 137.9°, 140.7°, and 107.5° for model A, B, D have obvious deviation to orthogonal situation and result in antiferromagnetic coupling constant *J*, −1.37, −0.14, and −0.13 cm^{-1}, respectively. For the $3d^8$ electronic configuration of Ni^{2+} ion in octahedral environment, only e_g orbitals are occupied by spin unpaired electrons with the torsion angle of N−Ni−Ni−N 180°, so the magnetic orbitals with $d_{x^2-y^2}$ character can overlap effectively and produce a larger *J* value −3.16 cm^{-1}. These results are also consistent with the prediction of Goodenough−Kanamori rules.[42]

In order to further understand the magnetic coupling interaction with hydrazine bridge, the changes of magnetic coupling constant *J* under different bond angles (M−N−N) and torsion angles (M−N−N−M) are also examined using DFT+BS method. Hampered by the steric hindrance of the coligand in **4·Mn,** the calculations are carried out in a limited structural region (Figure 8). The bond angle of Mn−N−N changed from 105.7 to 125.7 degree and the torsion angle of Mn−N−N−Mn changed from 82.9 to 178.9 degree. The resultant data show that the values of *J* stay negative and change little with the bond angles (Mn−N−N), but change larger with the torsion angles (Mn−N−N−Mn). Especially, the magnetic interaction turns to ferromagnetic coupling when the torsion angle decreases below 87.9° for the accidental orthogonality of two e_g orbitals occurred. This change confirms the discussions above that effective overlap of magnetic orbital is the source of antiferromagnetic coupling interaction. The situation is similar with our former studies on the EE-azido Bridged Ni^{2+}.[40]

(42) (a) Goodenough, J. B. *Phys. Rev.* **1955**, *100*, 564. *J. Phys. Chem. Solids* **1958**, *6*, 287. (b) Goodenough, J. B. *Magnetism and the Chemical Bond*; Interscience: New York, 1963. (c) Kanamori, J. *J. Phys. Chem. Solids* **1959**, *10*, 87.

Conclusions

Six transition metal sulfates containing hydrazine were obtained employing the hydrothermal method. These six complexes contain only hydrazine and sulfate ligand, but they have different structures because hydrazine and sulfate ligand act as different coordination modes. Compounds **1**−**3** are isomorphous with one-dimensional infinite chain but **4**−**6** are isomorphous with three-dimensional framework.

In summary, this is the first systematic study of magnetic properties of transition metal sulfates containing hydrazine until now. These six complexes all exhibit overall AF coupling between M^{2+} ions, which indicate that not only hydrazine but also sulfate transmits antiferromagnetic coupling. However, because of the difference of single-ion anisotropy and crystal structures, their magnetic properties differ at low temperatures: compounds **2**−**4** show antiferromagnetic order with the Néel temperatures 4.5, 4.5, and 7.5 K respectively. Compound **5·Co** is a weak ferromagnet due to spin canting and Compound **6·Ni** is a hidden spin-canted weak ferromagnet. The Curie temperatures for **5·Co** and **6·Ni** are 2.5 and 12.8 K, respectively. Both the calculated and the fitted *J* values from experimental data indicate consistently that the antiferromagnetic coupling between transition metal ions occurs through hydrazine (N_2H_4) and sulfate (SO_4^{2-}) bridging ligands. Furthermore, the magnetic coupling mechanism of hydrazine bridge are also examined using DFT+BS method. The resultant data show that the values of magnetic coupling constant *J* change little with the bond angles (Mn−N−N), but change larger with the torsion angles (Mn−N−N−Mn). Especially, the magnetic interaction could turn from antiferromagnetic to ferromagnetic coupling if the torsion angle decreases below 87.9° for the accidental orthogonality of two e_g orbitals occurred. Although the magnetic coupling is not as strong as that mediated by the other two-atom bridges such as CN^-, this work provides an unprecedented series for studying the coordination chemistry and magnetic properties of hydrazine complexes, and further enriches the field of molecule-based magnetic materials.

Acknowledgment. This work was supported by the NSFC (20821091, 90922033, 21071008) and the National Basic Research Program of China (2006CB601102, 2009CB929403).

Supporting Information Available: CIF files for **2**−**5**, scheme showing preparation of Btr, figures showing powder X-ray diffraction patterns, FTIR spectra, structures of compound **4**−**6**, and $1/\chi$ versus *T* plots, and a table showing the geometries of the N−H···O hydrogen bonds. This material is available free of charge via the Internet at http://pubs.acs.org.